Article

Dual-Wavelength Ratiometric Electrochemiluminescence Immunosensor for Cardiac Troponin I Detection

Jing Ye, Liping Zhu, Mengxia Yan, Qiuju Zhu, Qingqing Lu, Jianshe Huang, Hua Cui, and Xiurong Yang

Anal. Chem., **Just Accepted Manuscript** • DOI: 10.1021/acs.analchem.8b04640 • Publication Date (Web): 14 Dec 2018

Dual–Wavelength Ratiometric Electrochemiluminescence Immunosensor for Cardiac Troponin I Detection

Jing Ye,[†] Liping Zhu,[†] Mengxia Yan,[†,‡] Qiuju Zhu,[†] Qingqing Lu,[‡,§] Jianshe Huang,[‡] Hua Cui*[,†] and Xiurong Yang*[,†,‡,§]

[†] Department of Chemistry, University of Science and Technology of China, Hefei, Anhui 230026, P. R. China

[‡] State Key Laboratory of Electroanalytical Chemistry, Changchun Institute of Applied Chemistry, Chinese Academy of Sciences, Changchun, Jilin 130022, China

[§] University of Chinese Academy of Sciences, Beijing 100049, China

* Fax: +86 431 85689278. E-mail: xryang@ciac.ac.cn, hcui@ustc.edu.cn

ABSTRACT: Ratiometric electrochemiluminescence (ECL) has attracted special focus in biological analysis field because it could eliminate the environmental interference to gain precise measurement. Herein, a dual–wavelength ratiometric ECL biosensor was designed for detection of cardiac troponin I (cTnI), where (4,4'–dicarboxylicacid–2,2'–bipyridyl) ruthenium(II) ($Ru(dcbpy)_3^{2+}$) and Au nanoparticles loaded graphene oxide/polyethyleneimine (GPRu–Au) nanomaterial acts as an acceptor, and Au nanoparticles modified graphitic phase carbon nitride nanosheets composite (Au–CNN) acts as donor. Au–CNN shows high and steady ECL signal centered at 455 nm, which is well matched with the adsorption of GPRu–Au, thereby a high efficient electrochemiluminescent resonance energy transfer (ECL–RET) sensing platform is designed. AuNPs facilitate the immobilization of antibody on the nanomaterials through Au–N bond. The high surface area of graphene oxide/polyethyleneimine allows a large number of $Ru(dcbpy)_3^{2+}$ to be loaded, which immensely amplify the ECL signal. This sensing platform exhibits outstanding analytical performance toward cTnI with a detection limit of 3.94 fg/mL (S/N=3). The high reliability, selectivity and sensitivity of this ratiometric ECL biosensor provides a versatile sensing platform for the bioanalysis.

Among the causes of high cardiovascular mortality across the world, acute myocardial infarction (AMI) accounts for the primary proportion.[1] Therefore, timely diagnosis is essentially important before the onset of AMI.[2] At present, the clinical diagnosis mainly counts on the characteristic electrocardiogram evolution and the dynamic changes of serum biomarkers.[3] The common biomarkers for myocardial infarction include troponin (cTnI, cTnT and cTnC), creatine kinase, myoglobin copeptin and miRNA (miR–21, miR–499, miR–133a and miR208–a).[4,5] Among those biomarkers, cTnI (molecular weight 24 kDa) not only has excellent cardiac specificity, but also can provide a long detecting window for cardiac injury, which has been acknowledged as the most principal biomarker for AMI.[6,7] Recently, various methods have been designed to detect cTnI, including surface–enhanced raman spectroscopy,[8] colorimetric,[9] fluorescence,[10] electrochemical,[11] photochemical,[12] and electrochemiluminescence (ECL).[13] Compared to other methods, ECL shows high sensitivity and wide detecting range.[14,15] Several ECL assays for cTnI analysis have been developed. For example, Li et al. used luminol functionalized gold nanoparticles (AuNPs) to build a signal–off ECL biosensor.[16] Jo et al. combined triethanolamine functioned AuNPs with $Ru(bpy)_3^{2+}$–doped silica to form a signal–on ECL imunosensor.[17] However, the "off" or "on" ECL method rely on single emitter and signal. Some factors such as environmental changes would disturb real signal and cause false positive response in ECL analysis.[18,19] Inspired by ratiometric fluorescent method, ratiometric ECL method was put forward to tackle this challenge.[20]

Ratiometric ECL assays use the ratio of two signals from two emitters to establish a linear relationship, which could eliminate outside interferences to improve reliability of the detection.[21] Summing up, ratiometric ECL biosensor in terms of designing principles could be divided into two types: one type is dual–potential biosensor along with two emitters which character potential–dependent feature.[22] Zhang and his partners built the first dual–potential ECL sensor in 2013 by using luminol as anodic emitter and CdS quantum dots (QDs) as cathodic emitter.[23] Lei et al. construct a dual–potential biosensor with two novel emitters including O_2 and amino–terminated perylene derivative.[24] Chen et al. designed a potential–resolved biosensor, in which QDs acted as cathodic emitter and polymer dots acted as anodic one.[25] Generally, dual–potential sensor needs a pair of anodic/cathodic emitters which have independent luminescent ability, requiring broader potential range. The requirement strongly restricts the selection of two well–matched emitters and shared coreactant.[18,26] The other type is dual–wavelength biosensor. Feng and coworkers designed

the first dual–wavelength sensor in 2016, thus expanding the application of ECL technique.[27] Later, Zhou et al used silver nanoclusters which showed strong ECL emission and $Ru(bpy)_3^{2+}$ derivative which showed zero–like emission at cathodic potential, to construct a dual–wavelength immunosensor to determine apolipoprotein–A1.[28] Dual–wavelength biosensor integrates two wavelength–dependent emitters in one system to associate their intensities by electrochemiluminescent resonance energy transfer (ECL–RET). Dual–wavelength electrochemiluminescence could be completed at a narrower range of potential, avoid the limitation of one shared coreactant, and make a convincing results.[18] However, limited by the ECL intensity and wavelength, dual–wavelength technique has not been developed as widely as dual–potential.[29] Herein, we proposed a dual–wavelength ratiometric ECL method to detect cTnI with gold nanoparticles (AuNPs) functioned carbon nitride nanosheets (Au–CNN) as donor, graphene oxide/ polyethyleneimine/$Ru(dcbpy)_3^{2+}$/AuNPs (GPRu–Au) hybrid as accepter and potassium persulfate ($K_2S_2O_8$) as the shared coreactant.

Carbon nitride nanosheets (CNN), nontoxic and stable metal–free semiconductor, have been proved as a desirable cathodic ECL emitters with $K_2S_2O_8$ as coreactant.[30] However, the intrinsic low electrical conductivity of CNN limits its application in electrochemical and ECL analysis.[31] Therefore, introducing AuNPs into CNN, termed Au–CNN, not only increase the conductivity of the hybrid material and subsequently enhance ECL emission, but also facilitate the immobilization of primary antibody (pA).[29] $Ru(dcbpy)_3^{2+}$ molecules are covalently linked to polyethyleneimine (PEI) modified graphene oxide nanosheets through amido bond,[32] then AuNPs are loaded to form GPRu–Au hybrid. This design greatly enhances the loading amount of emitter and is beneficial to load capture antibody (cA).[33] Based on the ECL–RET between Au–CNN and GPRu–Au hybrid, a dual–wavelength ratiometric ECL immunoassay is designed for the determination of cTnI.[34] The preparation of GPRu–Au hybrid and the fabrication of the immunosensor are demonstrated in Scheme 1. This sandwich–type ECL–RET sensing platform performs ultrasensitive and accurate cTnI analysis, providing a sensing platform for diverse target proteins in bioanalysis field.

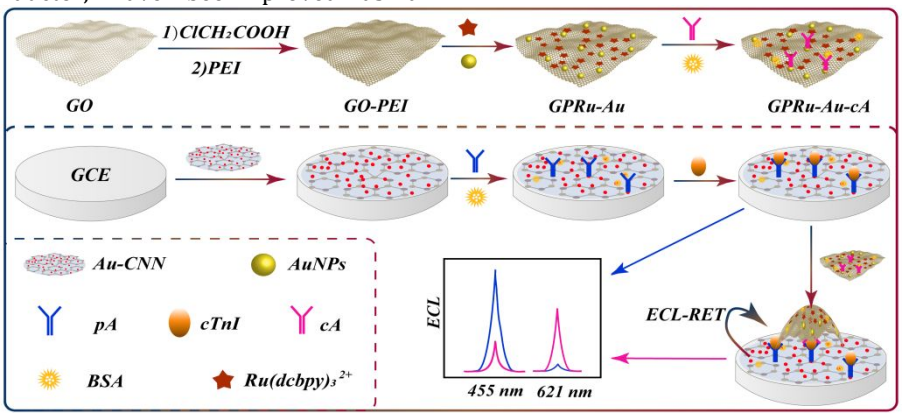

Scheme 1. Schematic Illustration for the preparation of GPRu–Au hybrid and the fabrication of the immunosensor.

EXPERIMENTAL SECTION

Reagents. Tris(4,4'–dicarboxylicacid–2,2'–bipyridyl) ruthenium (II) dichloride ($Ru(dcbpy)_3Cl_2$) was obtained from SunaTech Inc. (Suzhou, China). Bovine serum albumin (BSA), N–(3–(dimethylamino)propyl)–N'–ethylcarbodiimide hydrochloride (EDC), N–hydroxy succinimide (NHS), branched polyethylenimine (PEI, 25kDa), Chloroauric acid ($HAuCl_4{\cdot}3H_2O$), potassium ferrocyanide ($K_4[Fe(CN)_6]$) and potassium ferricyanide ($K_3[Fe(CN)_6]$) were bought from Sigma Aldrich (St. Louis, MO). Graphene oxide (1 mg/mL) was obtained from XFNANO INC (Nanjing, China). The cTnI, primary antibody (pA) and capture antibody (cA) were purchased from Abcam (Cambridge, MA). Clinical human serum samples were obtained from the Second Hospital of Jilin University (Changchun, China). Double–distilled (DI) water was privied by the Milli–Q water system (18.25 MΩ).

Apparatus. Transmission electron microscope (TEM) images were obtained by H–600 (Hitachi, Tokyo, Japan) and accelerating voltage was 100 kV. X–ray photoelectron spectroscopy (XPS) were surveyed on ESCALAB MK II spectrometer (VG Scientific) with Al Kα radiation. FT–IR spectra were acquired by Bruker VERTEX70 spectrometer in the range of 4000–500 cm^{-1} (Ettlingen, Germany). UV–vis absorption spectra were analyzed with Cary 50 UV–vis spectrophotometer (Varian). Zeta potential was measured with Zetasizer Nano ZS system (Malvern, England) at 25 °C ECL experiments were carried out with MPI–E ECL instrument (Xi'an, China), with photomultiplier tube (PMT) of 500 V, potential scan of 0 to –1.6 V and scan rate of 0.1 V/s. The experiments were done with a three–electrode system, composed of glassy carbon electrode (GCE, Φ=3 mm) as the working electrode, a platinum wire as the counter electrode and an Ag/AgCl as the reference electrode. The electrolyte of ECL measurement was PBS (0.1 M, pH 7.4) containing 0.1 M $K_2S_2O_8$.

Synthesis of Au–CNN. The CNN was prepared by liquid exfoliation method as described previously (details in Supporting Information)[29,35] For preparing Au–CNN, 20 μL of $HAuCl_4$ (0.01 M) was injected to 4 mL CNN solution,

stirring for 5 h at 25 °C. In succession, 50 μL of cold $NaBH_4$ (0.01 M) solution was dropped and kept stirring for 30 min with ice bath. Following 20 μL of sodium citrate (0.01 M) was added and further kept for 30 min at 37 °C. After centrifugation and washing, the precipitant was dissolved with 4 mL DI water to obtain Au–CNN.

Synthesis of GPRu–Au and the modification of capture antibody. The preparing procedures of GPRu–Au hybrid are demonstrated in Scheme 1. Carboxylated graphene oxide (GO–COOH) was obtained according to previously reported method (details in Supporting Information).[36] 4.5 mL of EDC (10 mg/mL) was added into 3.5 mL of GO–COOH (1 mg/mL). After 40 min, 3 mL of PEI (10 mg/mL) was added and kept stirring for 6 h. The resulting solution was performed a centrifugal operation at 10 000 rpm for 20 min. Afterwards, the unreacted material was removed after it was washed with DI water and then centrifuged three times. Finally, GO–PEI was dried in a vacuum oven. The resultant product was dissolved in DI water to prepare 1mg/mL GO–PEI.

GPRu–Au was synthesized by the following steps. First, 4.5 mg $Ru(dcbpy)_3^{2+}$ was dissolved in 5 mL DI water. Then, 14.4 mg EDC and 2.9 mg NHS were added under magnetic stirring for 1 h to activate the –COOH of $Ru(dcbpy)_3^{2+}$. Next, activated $Ru(dcbpy)_3^{2+}$ was reacted with 5 mL of GO–PEI for 2 h to synthesize GPRu. AuNPs was prepared according to the literature (Supporting Information).[37] Finally, 5 mL AuNPs solution was added into the mixture to prepare GPRu–Au hybrid based on the electrostatic force and interaction between Au-N bond. After centrifugated to remove excess reagents, GPRu–Au was transferred to 2 mL DI water for further use. 400 μL of capture antibody (cA, 10 μg/mL) was added into 2 mL of GPRu–Au solution and reacted overnight at 4 °C with stirring. And next 200 μL of BSA (1%) was mixed to block the nonspecific adsorption sites. After centrifugation, GPRu–Au–cA composite was obtained.

Fabrication of the ECL Biosensor. The GCE was polished with aluminum slurry (1.0, 0.3 and 0.05 μm), sonicated in distilled water and ethanol, and dried with nitrogen for next use. At first, 10 μL of Au–CNN suspension was modified on the cleaned GCE. After drying, 10 μL of pA (10 μg/mL) was dropped onto the modified GCE to react for 12 h at 4 °C. Then, 10 μL of BSA (1%) was placed to react for 1 h to block the excess active sites. Different concentration of cTnI was incubated for 40 min at 37 °C. Finally, 10 μL of GPRu–Au–cA bioconjugate was modified on the electrode through sandwiched immunoreaction for 60 min at 37 °C. Cleaning the modified electrode using three–times volume of PBS was performed after each modification step.

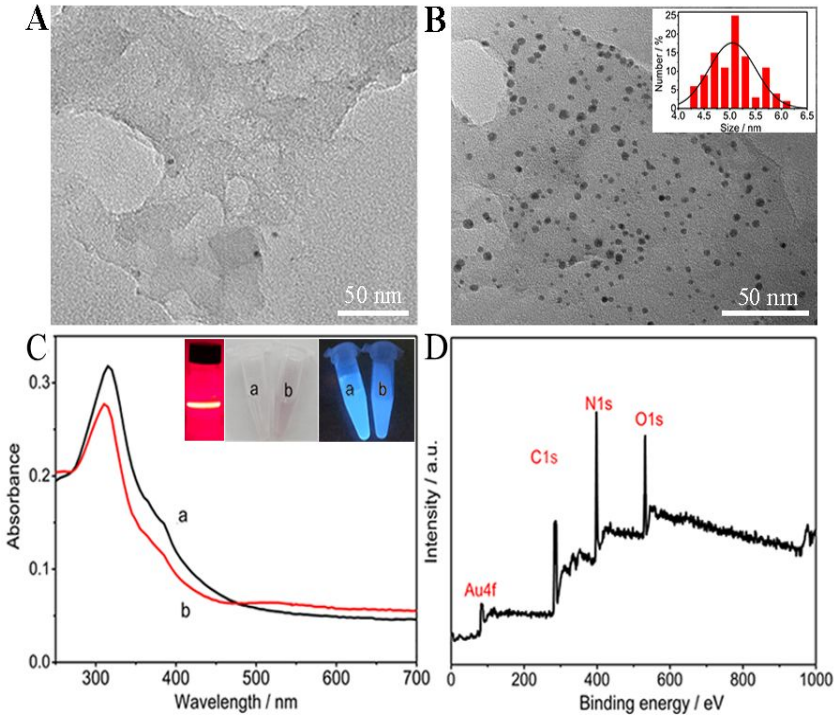

Figure 1. TEM images of (A) CNN and (B) Au–CNN. The inset was the size distribution of the AuNPs on Au–CNN. (C) UV–vis absorption spectra of (a) CNN and (b) Au–CNN. The insets from the left to right were Tyndall effect image of CNN solution, the photographs of CNN solution and Au–CNN solution under visible and ultraviolet light, respectively. (D) XPS spectrum of Au–CNN.

RESULTS AND DISCUSSION

Characterization of Au–CNN. A simple liquid exfoliation technique could be used to obtain the CNN according to foregoing work.[35] As showed in TEM image (Figure 1A), it showed a sheet–like morphology. Moreover, TEM image of Au–CNN indicated that synthesized nanoparticles were highly dispersed in the surface of CNN (Figure 1B). The approximately size of nanoparticles was about 5 nm (the inset in Figure 1B). The UV–vis absorption of CNN showed an absorption peak at 318 nm (Figure 1C, curve a). The Tyndall effect experiment (the left inset in Figure 1C) revealed that CNN solution characterized the

colloidal property and maintained steady in water for weeks.[35] Apart from the characteristic absorption peak of CNN, Au–CNN also had a small absorption peak at 520 nm (Figure 1C, curve b), which could be attributable to AuNPs, confirming that AuNPs had grown in the surface of CNN. Besides, the photograph of Au–CNN under visible light exhibited a little pink color also proved the presence of AuNPs (the middle inset in Figure 1C). The CNN and Au–CNN showed similar blue fluorescence under ultraviolet light (the right inset in Figure 1C). X–ray photoelectron spectroscopy (XPS) could be measured to illustrate the contained elements of samples. As seen from Figure 1D, the peaks at 83, 284, 399 and 532 eV were assigned to Au4f, C1s, N1 s and O1s, indicating Au–CNN mainly composed of C, N, O and Au elements, further acknowledging the successful synthesis of Au–CNN material.[38,39]

Characterization of GPRu–Au. TEM image proved that AuNPs have been anchored on the GPRu hybrid (Figure 2A). The size of AuNPs was about 13 nm (the inset in Figure 2A). UV–vis absorption spectra in Figure 2B were used to confirm the composition of GPRu–Au hybrid. The characteristic peaks of GO and AuNPs were measured to be 234 nm (curve a) and 520 nm (curve d), respectively. The corresponding absorption peak could be observed in GPRu–Au composite (curve e) and the weaker absorption performance was due to the combination of AuNPs increased the background absorbance. PEI had no obvious absorption peak in the measured wavelength range (curve b). And the $Ru(dcbpy)_3^{2+}$ showed two peaks in 297 and 478 nm (curve c), owing to the structure of carboxyl groups and bipyridyl rings, respectively.[40] Moreover, from what the magnified inset indicated, the two peaks of 479 nm and 520 nm in the absorption spectra of GPRu–Au composite (curve e) could be attributed to $Ru(dcbpy)_3^{2+}$ and AuNPs, respectively. The slight red–shift of $Ru(dcbpy)_3^{2+}$ could be attributed to the formation of amide, indicating the covalently interaction of $Ru(dcbpy)_3^{2+}$ and PEI.

The IR spectra provided further evidence for the preparation of GPRu–Au hybrid (Figure 2C). GO presented peaks at 3428, 1730, and 1624 cm^{-1} assigning to –OH, C=O, C=C stretching vibration (curve a).[41,42] Comparing with GO, two obvious peaks at 2918 and 2852 cm^{-1} were observed in PEI (curve b), GO–PEI (curve c) and GPRu–Au (curve d), which were corresponding to stretching vibration of $-CH_2$ of the PEI chains.[43] Additionally, GO-PEI showed two characteristic vibrations of amide I (1643 cm^{-1}) and amide II (1607 cm^{-1}). GPRu–Au hybrid showed obvious decrease in the peak of 1734 cm^{-1} and appeared an increased band at 1630 cm^{-1}, inferring that some carboxyl had been converted into amide.[44] Comparing to GO–PEI, GPRu–Au showed relatively high amide component, which could be attributed to the introduction of $Ru(dcbpy)_3^{2+}$. XPS survey spectrum of GPRu–Au showed the peaks at 84.5, 284, 399, 475 and 532 eV, which were assigned to Au4f, C1s, N1s, Ru3p and O1s, respectively (Figure 2D).[45] The deconvoluted high–resolution Au4f peak showed doublet at 82.7 ($Au4f_{7/2}$) and 86.4 eV ($Au4f_{5/2}$) (Figure S–1). The spin–orbit splitting of doublet components was 3.7 eV, which indicated the existence of zero valent gold.[46] The IR and XPS results verified that the GPRu–Au was successfully prepared.

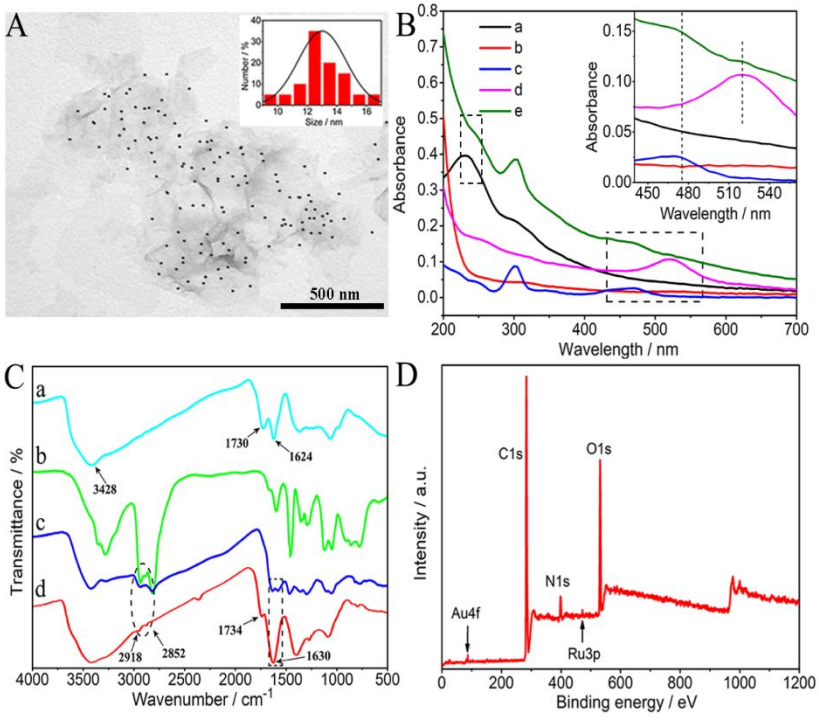

Figure 2. (A) TEM characterization of GPRu–Au. The inset was the size distribution of the AuNPs on GPRu–Au. (B) UV–vis absorption spectra of (a) GO, (b) PEI, (c) $Ru(dcbpy)_3^{2+}$, (d) AuNPs, and (e) GPRu–Au. (C) FI–IR spectra of (a) GO, (b) PEI, (c) GO–PEI and (d) GPRu–Au. The inset was the magnified image within the right dashed line rectangle. (D) XPS spectrum of GPRu–Au.

Additionally, the surface charges were measured for further charactering the synthetic process of GPRu–Au hybrid (Figure S–2). The zeta potentials of GO and GO–COOH were measured to be –38.4 and –47.3 mV, respectively. When GO interacted with positive PEI, the zeta potential dramatically changed from negative potential (–47.3 mV) to positive potential (39.4 mV), confirming the successful functionalization of PEI onto the surface of GO.[43,47] After GO–PEI further covalently combined with $Ru(dcbpy)_3^{2+}$, the zeta potential slight moved toward positive direction from 39.4 to 43.0 mV. Finally, the zeta potential of GPRu–Au was determined to be 21.5 mV, which attributed to the electrostatic combination between positively charged GPRu and negatively charged AuNPs (–58 mV).

Characterization of the stepwise fabrication of the ECL biosensor. Cyclic voltammetry (CV) and electrochemical impedance spectroscopy (EIS) were used to characterize the surface feature of the modified electrode.[13,48] The bare electrode showed a pair of symmetric–like redox peaks (Figure 3A, curve a).[22] After modified with the Au–CNN, an obvious decrease in redox peak was observed (curve b). When pA (curve c), BSA (curve d) and cTnI (curve e) were successively assembled into the electrode, a concomitant decreasing trend of the redox peaks was observed. This phenomenon was attributed to the non–conducing proteins which impeded the electron transfer at the electrode interface. Finally, there was a slight increase of redox current when GPRu–Au was attached onto the modified electrode (curve f), which was due to the good conducting power of GPRu–Au hybrid. As shown in Figure 3B, EIS results demonstrated that the charge transfer resistance (R_{et}) gradually increased with stepwise assembling the immunosensor (curve a–e). However, when GPRu–Au was immobilized onto the modified electrode (curve f), the R_{et} obviously decreased. Au-CNN showed a high ECL intensity when dropped onto electrode (Figure 3C, curve b). When pA (curve c), BSA (curve d) and cTnI (curve e) were successively assembled into the GCE, slightly reductions were observed. When GPRu–Au–cA dropped onto the electrode, the ECL intensity raised a bit (curve f), indicating successful modification of GPRu–Au–cA. These results were in conformity with CV and EIS, confirming the successful fabrication of the proposed ECL immunosensor.

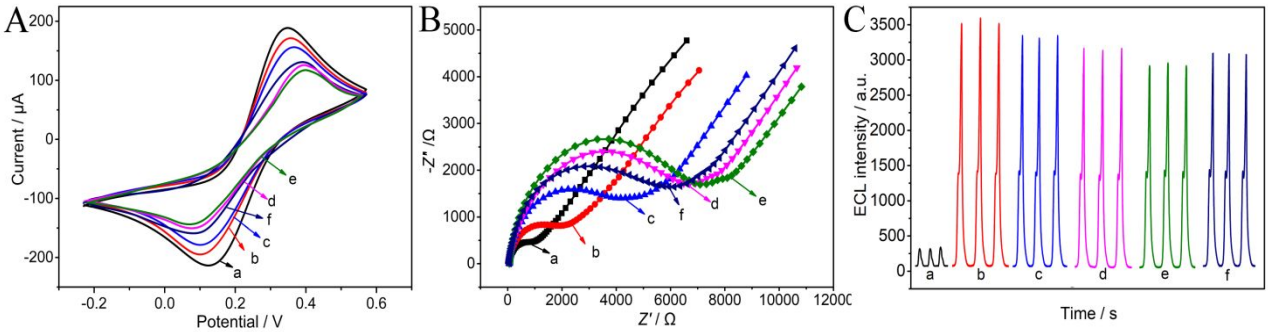

Figure 3. (A) CV, (B) EIS characterization and (C) ECL responses for the stepwise fabrication of immunosensor. (a) bare GCE, (b) Au–CNN/GCE, (c) pA/Au–CNN/GCE, (d) BSA/pA/Au–CNN/GCE, (e) cTnI/BSA/pA/Au–CNN/GCE, (f) GPRu–Au–cA/ cTnI/BSA/pA/Au–CNN/GCE. Concentration for cTnI,1 pg/mL; electrolyte, PBS (0.1 M, pH 7.4) containing 10 mM $[Fe(CN)_6]^{3-}/[Fe(CN)_6]^{4-}$ electroactive probe; scan rate for CV, 100 mV/s; frequency for EIS, 0.1–10^5 Hz; PMT for ECL, 300 V.

The ECL–RET mechanism of ratiometric ECL sensor. The proposed immunosensor was dependent on the ECL–RET between Au–CNN and GPRu–Au. The ECL intensity of bare GCE, CNN, Au–CNN and GPRu–Au modified electrodes were evaluated firstly in order to illustrate the mechanism, (Figure 4A). No ECL signal can be observed at the bare GCE (curve a). And CNN modified electrode showed weak ECL response with the onset and peak potential at –1.1 V and –1.25 V, respectively (curve c). Au–CNN exhibited greatly enhanced ECL emission at the same potential comparing to CNN (curve d), which is due to electrocatalytic reduction of $S_2O_8^{2-}$ by AuNPs.[31] Therefore, Au–CNN can be used as an excellent ECL donor. The ECL mechanism of Au–CNN/$S_2O_8^{2-}$ has been reported in previously report (equation 1–4).[29,49] When the electrode was scanned in cathodic potential, the CNN and $S_2O_8^{2-}$ were reduced to $Au–CNN^{\bullet-}$ and $SO_4^{\bullet-}$ (equation 1–2), respectively. The strong oxidant $SO_4^{\bullet-}$ could react with $Au–CNN^{\bullet-}$ to produce excited state $Au–CNN^*$(equation 3), which would generate strong emission at 455 nm when returned to ground state (equation 4). However, the GPRu–Au hybrid modified GCE showed very weak ECL response under the same conditions (curve b), suggesting that GPRu–Au itself can't be a well ECL emitter in this cathodic ECL system.[50]

$$Au–CNN + e^- \rightarrow Au–CNN^{\bullet-} \quad (1)$$

$$S_2O_8^{2-} + e^- \rightarrow SO_4^{2-} + SO_4^{\bullet-} \quad (2)$$

$$Au–CNN^{\bullet-} + SO_4^{\bullet-} \rightarrow Au–CNN^* + SO_4^{2-} \quad (3)$$

$$Au–CNN^* \rightarrow Au–CNN + h\nu\ (455\ nm) \quad (4)$$

As shown in Fugure 4B, it can be seen that the UV–vis spectra of GPRu–Au hybrid (curve a) had matched spectral overlap with the ECL emission spectra of Au–CNN centered at 455 nm (curve b), indicating that the energy transfer from Au–CNN donor to GPRu–Au acceptor could occur. We also investigated the ECL spectra of the immunosensor at different cTnI concentration by using a series of optical filter (Figure 4C). In the absence of cTnI, only Au–CNN emission peak at 455 nm was observed (curve a). With the increase of cTnI concentration, however, the ECL emission intensity of Au–CNN

continuously decreased, accompanying by the significantly increase in GPRu–Au emission at 621 nm (curve b–d).

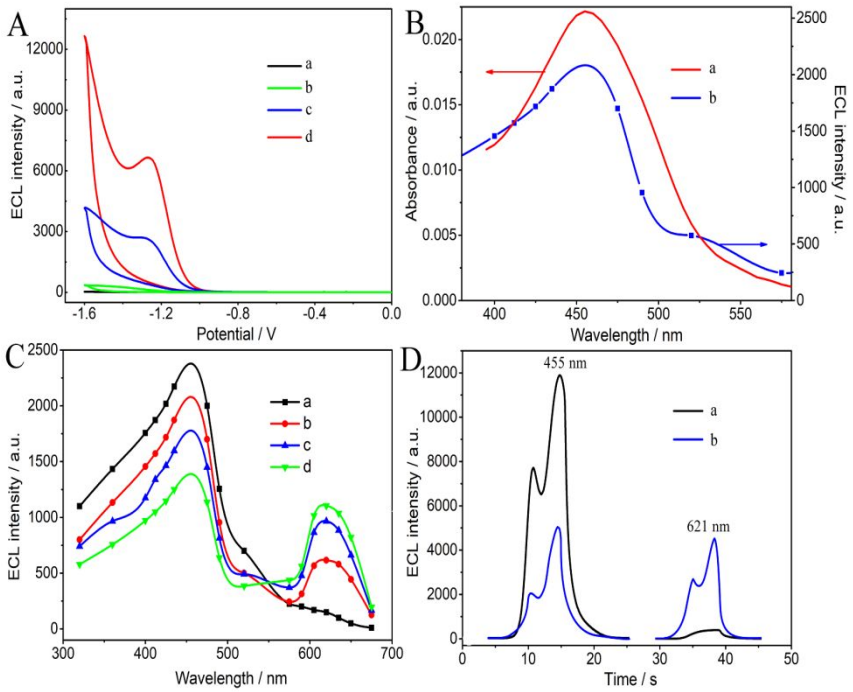

Figure 4. (A) ECL–potential plots of (a) bare GCE, (b) GPRu–Au/GCE, (c) CNN/GCE and (d) Au–CNN/GCE. (B) (a) UV–vis absorption of GPRu–Au, (b) ECL spectrum of Au–CNN/GCE. (C) ECL emission spectra of GPRu–Au–cA/cTnI /BSA/pA/Au–CNN/GCE in different cTnI concentration: (a) 0, (b) 1 pg/mL, (c) 100 pg/mL and (d) 1 ng/mL. The ECL spectra were gained through a series of optical filter. (D) The ECL responses at 455 nm and 621 nm of (a) cTnI/BSA/pA/Au–CNN/GCE, (b) GPRu–Au–cA/cTnI/BSA/pA/Au–CNN/GCE. Concentration for cTnI, 1 ng/mL.

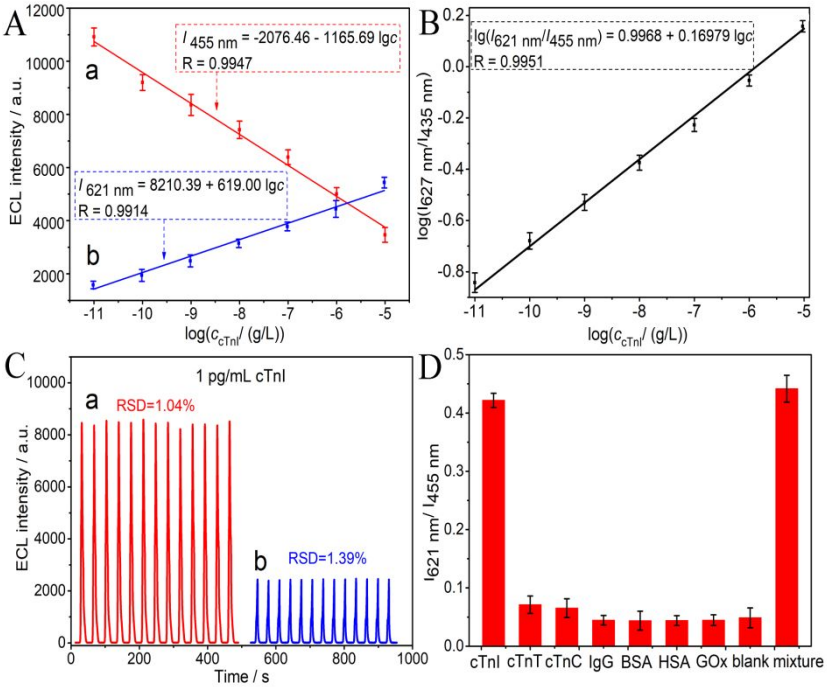

Figure 5. (A) Relationship between the ECL signal at wavelength of (a) 455 nm or (b) 621 nm and the logarithm of cTnI concentration. A series of cTnI concentration were 10 fg/mL, 100 fg/mL, 1 pg/mL, 10 pg/mL, 100 pg/mL, 1 ng/mL and 10 ng/mL. (B) The calibration curve for cTnI determination. (C) ECL reproducibility at wavelength of (a) 455 nm and (b) 621 nm with 1 pg/mL cTnI under continuous 13 cycles of cyclic voltammetry (D) ECL selectivity of the immunosensor against cTnI (10 pg/mL) and other nonspecific proteins (100 pg/mL).

The ECL responses before and after modified with GPRu–Au at both wavelengths were investigated to further confirm the ECL–RET (Figure 4D). After the assembly of GPRu–Au, the ECL intensity of Au–CNN greatly reduced at 455 nm, at the same time, a strong ECL peak of GPRu–Au appeared at 621 nm. Alone GPRu–Au exhibited very weak ECL emission (Figure 4A, curve b), therefore the enhanced ECL intensity at 621 nm must be arose from the ECL–RET of Au–CNN emission. All these results indicated the effective ECL–RET between Au–CNN and GPRu–Au and the feasibility of our designed sensing platform.

Detection of cTnI with the Biosensor. The effects of the concentration of pA, as well as the incubation time of cTnI and GPRu–Au–cA on the ECL responses were investigated to optimize the analytical performance of the immunosensor (Figure S–3). Under the optimum conditions of 10 μg/mL pA concentration, 40 min cTnI incubation time and 60 min GPRu–Au–cA incubation time, the dual–wavelength ratiometric system was used to quantitatively determine the concentration of the cTnI. With the increase of cTnI concentration, a lot GPRu–Au hybrids were modified onto the electrode by sandwich assay. Therefore, the ECL signal from Au–CNN (455 nm) reduced and that from ECL-RET (621 nm) raised (Figure 5A). To obtain a better ECL reliability, we utilized the ratiometric measurement to determine cTnI by counting the ratio of $I_{455\ nm}$ and $I_{621\ nm}$.[28] The logarithm of ratio was linearly dependent on the logarithmic value of cTnI concentration in the concentration range from 10 fg/mL to 10 ng/mL (Figure 5B). The correlation coefficient of calibration curve was 0.9951. The detection limit (LOD) of ratiometric biosensor was as low as 3.94 fg/mL (S/N=3). Our immunosensor exhibits comparable or a wider detection range and lower LOD compared with previously reported biosensors for cTnI detection (Table S–1).

Reproducibility and Selectivity of the Biosensor. The ECL response for progressive potential scanning of 13 cycles was recorded (Figure 5C). The relative standard deviation (RSD) of ECL intensity at 455 nm and 621 nm were 1.04% and 1.39%, respectively, demonstrating excellent reproducibility of the proposed ECL system. Some nonspecific proteins, including cTnT, cTnC, IgG, BSA, HSA and GOx, were chosen as interference proteins to evaluate the selectivity of the ECL immunosensor. As shown in Figure 5D, the mixture of cTnI and nonspecific proteins had similar result with pure cTnI, and nonspecific proteins showed almost identical response to that of the blank sample, highlighting the excellent specificity of the biosensor.

Detection of cTnI in human serum sample. Different concentrations of cTnI were spiked in 2% or 5% real human serum, and then detected with the proposed immunosensor. The detecting result, recovery and RSD of cTnI were showed in Table S-2. The recovery values were ranging from 93.80% to 105.62% and RSD values of three times detection were less than 2%, indicating that our proposed dual–wavelength ratiometry ECL biosensor has potential of cTnI detection in real biological samples.

CONCLUSIONS

In this work, a dual–wavelength ratiometric ECL–RET immunosensor was designed to detect biomarker cTnI, with Au–CNN as donor and GPRu–Au as acceptor. Benefiting from the high ECL–RET efficiency between Au–CNN and GPRu–Au, the immunosensor showed high sensitivity with a limit of detection 3.94 fg/mL (S/N=3), and wide linear range from 10 fg/mL to 10 ng/mL. Besides, this immunosensor also exhibited good reproducibility and selectivity for the detection of cTnI. By introducing the corresponding antibody, this sensing platform could easily be extended for the determination of different target proteins.

ASSOCIATED CONTENT

Supporting Information

The Supporting Information is available free of charge on the ACS Publications website.

Preparation of CNN, GO-COOH and AuNPs, deconvoluted high–resolution XPS spectra of Au4f of GPRu–Au (Figure S–1), the zeta potential which characterized the the synthetic process of GPRu–Au hybrid (Figure S–2), optimization of the modification conditions (Figure S–3), comparison of the performance of several typical cTnI biosensors (Table S–1), results of cTnI concentration in the analysis of human serum samples (Table S-2).

AUTHOR INFORMATION

Corresponding Author

*E-mail: xryang@ciac.ac.cn. Tel.: +86 431 85262056; Fax: +86 431 85689278.

*E-mail: hcui@ustc.edu.cn. Tel: +86 0551 63600730. Fax: +86 0551 63600730.

Author Contributions

The manuscript was written through contributions of all authors.

Notes

The authors declare no competing financial interest.

ACKNOWLEDGMENT

This work was supported by the National Key Research and Development Program of China (2016YFA0201301), the National Natural Science Foundation of China (no. 21435005 and 21627808), Key Research Program of Frontier Sciences, CAS (QYZDY-SSW-SLH019).

REFERENCES

(1) Wu, Q.; Sun, Y.; Zhang, D.; Li, S.; Zhang, Y.; Ma, P.; Yu, Y.; Wang, X. H.; Song, D. Q. Ultrasensitive magnetic field-assisted surface plasmon resonance immunoassay for human cardiac troponin I. *Biosens. Bioelectron.* **2017**, *96*, 288-293.

(2) Tuteja, S. K.; Kukkar, M.; Suri, C. R.; Paul, A. K.; Deep, A. One step in-situ synthesis of amine functionalized graphene for immunosensing of cardiac marker cTnI. *Biosens. Bioelectron.* **2015**, *66*, 129-135.

(3) Han, X.; Li, S. H.; Peng, Z. L.; Othman, A. M.; Leblanc, R. Recent Development of Cardiac Troponin I Detection. *ACS Sens.* **2016**, *1*, 106-114.

(4) Han, Z. L.; Shu, J. N.; Jiang, Q. S.; Cui, H. Coreactant-Free and Label-Free Eletrochemiluminescence Immunosensor for Copeptin Based on Luminescent Immuno-Gold Nanoassemblies. *Anal. Chem.* **2018**, *90*, 6064-6607.

(5) Chen, A. Y.; Ma, S. Y.; Zhuo, Y.; Chai, Y. Q.; Yuan, R. In Situ Electrochemical Generation of Electrochemiluminescent Silver Naonoclusters on Target-Cycling Synchronized Rolling Circle Amplification Platform for MicroRNA Detection. *Anal. Chem.* **2016**, *88*, 3203-3210.

(6) Nandhikonda, P.; Heagy, M. D. An abiotic fluorescent probe for cardiac troponin I. *J. Am. Chem. Soc.* **2011**, *133*, 14972-14974.

(7) Akter, R.; Jeong, B.; Lee, Y. M.; Choi, J. S.; Rahman, M. A. Femtomolar detection of cardiac troponin I using a novel label-free and reagent-free dendrimer enhanced impedimetric immunosensor. *Biosens. Bioelectron.* **2017**, *91*, 637-643.

(8) Garza J. T.; Cote G. L. Collection Method of SERS Active Nanoparticles for Sensitive and Precise Measurements. *Anal. Chem.* **2017**, *89*, 13120-13127.

(9) Liu, X. H.; Wang, Y.; Chen, P.; McCadden, A.; Palaniappan, A.; Zhang, J. L.; Liedberg, B. Peptide Functionalized Gold Nanoparticles with Optimized Particle Size and Concentration for Colorimetric Assay Development: Detection of Cardiac Troponin I. *ACS Sens.* **2016**, *1*, 1416-1422.

(10) Lou, D. D.; Fan, L.; Cui, Y.; Zhu, Y. F.; Gu, N.; Zhang, Y. Fluorescent Nanoprobes with Oriented Modified Antibodies to Improve Lateral Flow Immunoassay of Cardiac Troponin I. *Anal. Chem.* **2018**, *90*, 6502-6508.

(11) Dhawan, S.; Sadanandan, S.; Haridas, V.; Voelcker, N. H.; PrietoSimón, B. Novel peptidylated surfaces for interference-free electrochemical detection of cardiac troponin I. *Biosens. Bioelectron.* **2018**, *99*, 486-492.

(12) Fan, D. W.; Bao, C. Z.; Khan, M. S.; Wang, C. L.; Zhang, Y.; Liu, Q. Z.; Zhang, X.; Wei, Q. A novel label-free photoelectrochemical sensor based on N,S-GQDs and CdS co-sensitized hierarchical Zn2SnO4 cube for detection of cardiac troponin I. *Biosens. Bioelectron.* **2018**, *106*, 14-20.

(13) Yang X.; Yu Y. Q.; Peng L. Z.; Lei Y. M.; Chai Y. Q.; Yuan R.; Zhuo Y. Strong Electrochemiluminescence from MOF Accelerator Enriched Quantum Dots for Enhanced Sensing of Trace cTnI. *Anal. Chem.* **2018**, *90*, 3995–4002.

(14) Liu, Z. Y.; Qi, W. J.; Xu, G. B. Recent advances in electrochemiluminescence. *Chem. Soc. Rev.* **2015**, *44*, 3117-3142.

(15) Hu, L.; Xu, G. Applications and trends in electrochemiluminescence. *Chem. Soc. Rev.* **2010**, *39*, 3275-3304.

(16) Li, F.; Yu, Y. Q.; Cui, H.; Yang, D.; Bian, Z. P. Label-free electrochemiluminescence immunosensor for cardiac troponin I using luminol functionalized gold nanoparticles as a sensing platform. *Analyst* **2013**, *138*, 1844-1850.

(17) Jo, H. H.; Gu, H.; Jeon, W.; Youn, H.; Her, J.; Kim, S. K.; Lee, J.; Shin, J. H.; Ban, C. Electrochemical aptasensor of cardiac troponin I for the early diagnosis of acute myocardial infarction. *Anal. Chem.* **2015**, *87*, 9869-9875.

(18) Wu, P.; Hou, X. D.; Xu, J. J.; Chen, H. Y. Ratiometric fluorescence, electrochemiluminescence, and photoelectrochemical chemo/biosensing based on semiconductor quantum dots. *Nanoscale* **2016**, *8*, 8427-8442.

(19) Cheng, Y.; Huang, Y.; Lei, J. P; Zhang, L.; Ju, H. X. Design and biosensing of Mg^{2+}-dependent DNAzyme-triggered ratiometric electrochemiluminescence. *Anal. Chem.* **2014**, *86*, 5158-5163.

(20) Lu, H. J.; Zhao, W.; Xu, J. J.; Chen, H. Y. Visual electrochemiluminescence ratiometry on bipolar electrode for bioanalysis. *Biosens. Bioelectron.* **2018**, *102*, 624-630.

(21) Wu, L.; Ding, F.; Yin, W. M.; Ma, J.; Wang, B. R.; Nie, A. X.; Han, H. Y. From Electrochemistry to Electroluminescence: Development and Application in a Ratiometric Aptasensor for Aflatoxin B1. *Anal. Chem.* **2017**, *89*, 7578-7585.

(22) Wang, Y. F.; Shan, D. L.; Wu, G. F.; Wang, H.; Ru, F.; Zhang, X. H.; Li, L. F.; Qian, Y. X.; Lu, X. Q. A novel "dual-potential" ratiometric electrochemiluminescence DNA sensor based on enhancing and quenching effect by G-quadruplex / hemin and Au-Luminol bifunctional nanoparticles. *Biosens. Bioelectron.* **2018**, *106*, 64-70.

(23) Zhang, H. R.; Xu, J. J.; Chen, H. Y. Electrochemiluminescence Ratiometry: A New Approach to DNA Biosensing. *Anal. Chem.* **2013**, *85*, 5321-5325.

(24) Lei, Y. M.; Huang, W. X.; Zhao, M.; Chai, Y. Q.; Yuan, R.; Zhuo, Y. Electrochemiluminescence Resonance Energy Transfer System: Mechanism and Application in Ratiometric Aptasensor for Lead Ion. *Anal. Chem.* **2015**, *87*, 7787-7794.

(25) Chen, H. M.; Zhang, H.; Yuan, R.; Chen, S. H. Novel Double-Potential Electrochemiluminescence Ratiometric Strategy in Enzyme-Based Inhibition Biosensing for Sensitive Detection of Organophosphorus Pesticides. *Anal. Chem.* **2017**, *89*, 2823-2829.

(26) Huang, Y.; Lei, J. P.; Cheng, Y.; Ju, H. X. Ratiometric electrochemiluminescent strategy regulated by electrocatalysis of palladium nanocluster for immunosensing. *Biosens. Bioelectron.* **2016**, *77*, 733-739.

(27) Wu, P.; Xu, C. Y.; Hou, X. D.; Xu, J. J.; Chen, H. Y. Dual-emitting quantum dot nanohybrid for imaging of latent fingerprints: simultaneous identification of individuals and traffic light-type visualization of TNT. *Chem. Sci.* **2015**, *6*, 4445-4450.

(28) Zhou, Y.; Yu, Y. Q.; Chai, Y. Q.; Yuan, R. Electrochemical synthesis of silver nanoclusters on electrochemiluminescent resonance energy transfer amplification platform for Apo-A1 detection. *Talanta* **2018**, *181*, 32-37.

(29) Feng, Q. M.; Shen, Y. Z.; Li, M. X.; Zhang, Z. L.; Zhao, W.; Xu, J. J.; Chen, H. Y. Dual-Wavelength Electrochemiluminescence Ratiometry Based on Resonance Energy Transfer between Au Nanoparticles Functionalized g-C_3N_4 Nanosheet and $Ru(bpy)_3^{2+}$ for microRNA Detection. *Anal. Chem.* **2016**, *88*, 937-944.

(30) Ji, J. J.; Wen, J.; Shen, Y. F.; Lv, Y. Q.; Chen, Y. L.; Liu, S. Q.; Ma, H. B.; Zhang, Y. J. Simultaneous Noncovalent Modification and Exfoliation of 2D Carbon Nitride for Enhanced Electrochemiluminescent Biosensing. *J. Am. Chem. Soc.* **2017**, *139*, 11698-11701.

(31) Chen, L. C.; Zeng, X. T.; Si, P.; Chen, Y. M.; Chi, Y. W.; Kim, D. H.; Chen, G. N. Gold nanoparticle-graphite-like C_3N_4 nanosheet nanohybrids used for electrochemiluminescent immunosensor. *Anal. Chem.* **2014**, *86*, 4188-4195.

(32) Yu, Y. Q.; Wang, J. P.; Zhao, M.; Hong, L. R.; Chai, Y. Q.; Yuan, R.; Zhuo, Y. Target-catalyzed hairpin assembly and intramolecular/intermolecular co-reaction for signal amplified electrochemiluminescent detection of microRNA. *Biosens. Bioelectron.* **2016**, *77*, 442-450.

(33) Lei, J. P.; Ju, H. X. Signal amplification using functional nanomaterials for biosensing. *Chem. Soc. Rev.* **2012**, *41*, 2122-2134.

(34) Jiang, J. J.; Chen, D.; Du, X. Z. Ratiometric electrochemiluminescence sensing platform for sensitive glucose detection based on in situ generation and conversion of coreactants. *Sens. Actuators, B* **2017**, *251*, 256-263.

(35) Zhang, X. D.; Xie, X.; Wang, H.; Zhang, J. J.; Pan, B. C.; Xie, Y. Enhanced photoresponsive ultrathin graphitic-phase C3N4 nanosheets for bioimaging. *J. Am. Chem. Soc.* **2013**, *135*, 18-21.

(36) Yu, Y. Q.; Zhou, M.; Shen, W.; Zhang, H. L.; Cao, Q.; Cui, H. Synthesis of electrochemiluminescent graphene oxide functionalized with a ruthenium(II) complex and its use in the detection of tripropylamine. *Carbon* **2012**, *50*, 2539-2545.

(37) Fu, Z. Y.; Zhou, X. M.; Xing, D. Sensitive colorimetric detection of Listeria monocytogenes based on isothermal gene amplification and unmodified gold nanoparticles. *Methods* **2013**, *64*, 260-266.

(38) Kong L. Q.; Ji Y. J.; Dang Z. Z.; Yan J. Q.; LI P.; Li Y. Y.; Liu S. Z. g-C_3N_4 Loading Black Phosphorus Quantum Dot for Efficient and Stable Photocatalytic H_2 Generation under Visible Light. *Adv. Funct. Mater.* **2018,** *28*, 1800668.

(39) Vazquez-Gonzalez, M.; Liao, W. C.; Cazelles, R.; Wang, S.; Yu, X.; Gutkin, V.; Willner, I. Mimicking Horseradish Peroxidase Functions Using Cu^{2+}-Modified Carbon Nitride Nanoparticles or

Cu^{2+}-Modified Carbon Dots as Heterogeneous Catalysts. *ACS Nano* **2017**, *11*, 3247-3253.

(40) Chen, A. Y.; Zhao, M.; Zhuo, Y.; Chai, Y. Q.; Yuan, R. Hollow Porous Polymeric Nanospheres of a Self-Enhanced Ruthenium Complex with Improved Electrochemiluminescent Efficiency for Ultrasensitive Aptasensor Construction. *Anal. Chem.* **2017**, *89*, 9232-9238.

(41) Wei, T. S.; Dong, T. T; Xing, H.; Liu, Y.; Dai, Z. H. Cucurbituril and Azide Cofunctionalized Graphene Oxide for Ultrasensitive Electro-Click Biosensing. *Anal. Chem.* **2017**, *89*, 12237-12243.

(42) Xue, M. Q.; Li, F. W.; Zhu, J. A.; Song, H.; Zhang, M. N.; Cao, T. B. Structure-Based Enhanced Capacitance: In Situ Growth of Highly Ordered Polyaniline Nanorods on Reduced Graphene Oxide Patterns. *Adv. Funct. Mater.* **2012**, *22*, 1284-1290.

(43) Zhang, L. M.; Lu, Z. X.; Zhao, Q. H.; Huang, J.; Shen, H.; Zhang, Z. J. Enhanced chemotherapy efficacy by sequential delivery of siRNA and anticancer drugs using PEI-grafted graphene oxide. *Small* **2011**, *7*, 460-464.

(44) Wang, H. B.; Zhang, Q.; Chu, X.; Chen, T. T.; Ge, J.; Yu, R. Q. Graphene oxide-peptide conjugate as an intracellular protease sensor for caspase-3 activation imaging in live cells. *Angew. Chem., Int. Ed.* **2011**, *50*, 7065-7069.

(45) Tao, Y.; Lin, Y. H.; Huang, Z. Z.; Ren, J. S.; Qu, X. G. Incorporating graphene oxide and gold nanoclusters: a synergistic catalyst with surprisingly high peroxidase-like activity over a broad pH range and its application for cancer cell detection. *Adv. Mater.* **2013**, *25*, 2594-2599.

(46) Zhu, Q. J.; Huang, J. S.; Yan, M. X.; Ye, J.; Wang, D. W.; Lu, Q. Q.; Yang, X. R. N-(Aminobutyl)-N-(ethylisoluminol)-functionalized gold nanoparticles on cobalt disulfide nanowire hybrids for the non-enzymatic chemiluminescence detection of H_2O_2. *Nanoscale* **2018**, *10*, 14847-14851.

(47) Feng, L. Z.; Yang, X. Z.; Shi, X. Z.; Tan, X. F.; Peng, R.; Wang, J.; Liu, Z. A. Polyethylene glycol and polyethylenimine dual-functionalized nano-graphene oxide for photothermally enhanced gene delivery. *Small* **2013**, *9*, 1989-1997.

(48) Fan, X. M.; Wang, S. M.; Li Z. J.; Jia, X. Y.; Zheng, X. W. Determination of Adenosine Based on $Ru(bpy)_3^{2+}$/AuNPs/SWCNTs/Adenosine Aptamer Electrochemiluminescence Sensor. *Chin. J. Anal. Chem.* **2017**, 45, 1353-1359.

(49) Cheng, C M..; Huang, Y.; Tian, X. Q.; Zheng, B. Z.; Li, Y.; Yuan, H. Y.; Xiao, D.; Xie, S. P.; Choi, M. M. Electrogenerated chemiluminescence behavior of graphite-like carbon nitride and its application in selective sensing Cu^{2+}. *Anal. Chem.* **2012**, *84*, 4754-4759.

(50) Yu, Y. C.; Lu, C.; Zhang, M. N. Gold Nanoclusters@$Ru(bpy)_3^{2+}$-Layered Double Hydroxide Ultrathin Film as a Cathodic Electrochemiluminescence Resonance Energy Transfer Probe. *Anal. Chem.* **2015**, 87, 8026-8032.

For TOC only

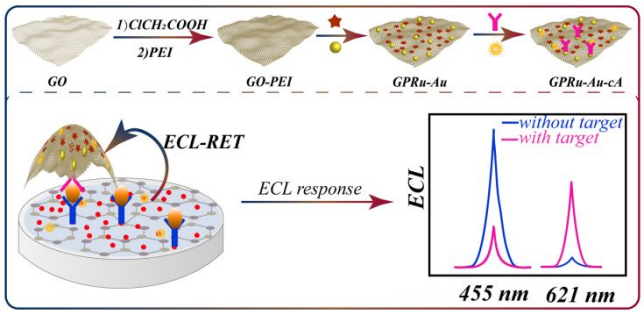
1)ClCH2COOH
2)PEI
GO
GO-PEI
GPRu-Au
GPRu-Au-cA
ECL-RET
ECL response
ECL
without target
with target
455 nm
621 nm